

Supporting information

TiO₂-B nanorods based competitive-like non-enzyme photoelectrochemical sensing platform for glucose noninvasive detection

Shupei Zhang^{#a}, Guifang Xu^{#a}, Lingshan Gong^a, Hong Dai^{a*}, Yilin Li^a, Zhensheng Hong^{b*}, Yanyu Lin^c

a College of Chemistry and Chemical Engineering, Fujian Normal University, Fuzhou 350108, P. R. China

b College of Physics and Energy, Fujian Normal University, Fujian Provincial Key Laboratory of Quantum Manipulation and New Energy Materials, Fuzhou 350108, P. R. China

c Ministry of Education Key Laboratory of Analysis and Detection for Food Safety, and Department of Chemistry, Fuzhou University, Fuzhou 350002, P. R. China

*Corresponding author

Fax: (+86)-591-83124888;

E-mail: dhong@fjnu.edu.cn (H. Dai);

winter0514@163.com (Z. Hong)

These authors equally contributed to this work.

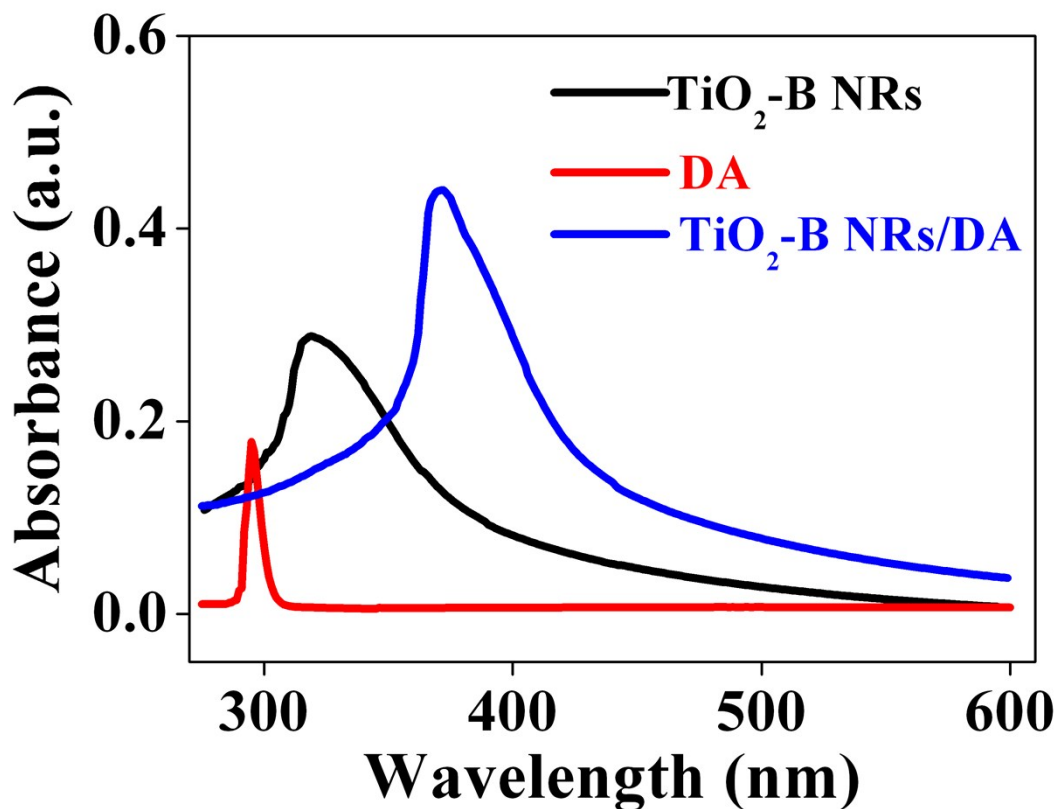


Figure S1. UV-vis spectra of the TiO₂-B NRs, DA and TiO₂-B NRs/DA.

To further explore the function of DA in this hybrid, UV-vis spectra of TiO₂-B NRs, DA and TiO₂-B NRs/DA were exhibited in Figure S1. Obviously, the absorption peak of the DA and TiO₂-B NRs appeared at 290 nm and 319 nm, respectively. As expected, both peaks of DA and TiO₂-B NRs almost disappeared and a new peak appeared at 380 nm in TiO₂-B NRs/DA film. Besides, the enhanced absorption in visible light region can be seen in the TiO₂-B NRs/DA film. This phenomenon is similar to the results in previous reports.^{14, S1-S2} Therefore, the improved photoelectrochemical performance of TiO₂-B NRs/DA was resulted from the DA-Ti charge transfer complex formed at the surface of TiO₂-B NRs, which the hybrid led to the large energy shift of valence band.^{14, S2-S4}

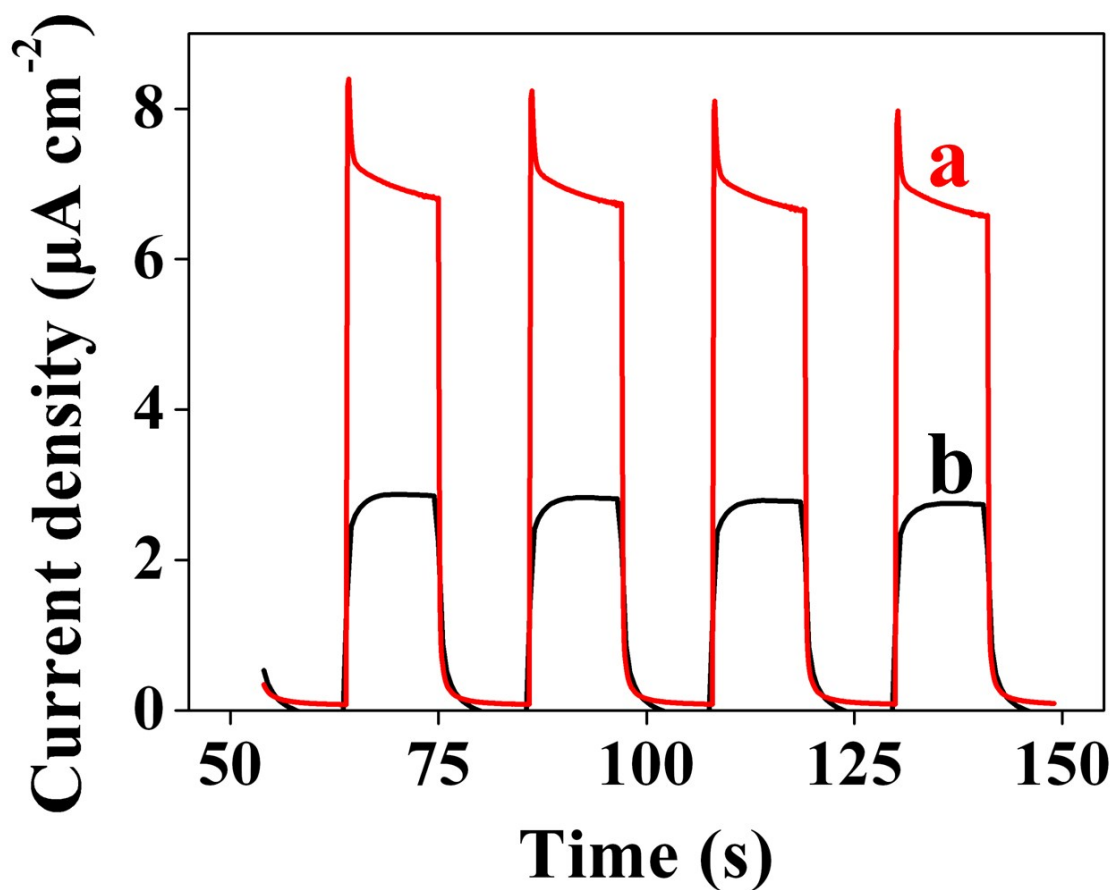


Figure S2. The photocurrent response of TiO₂-B NRs/DA in 0.1 M PBS without (a) and with (b) deaerated by pure nitrogen for 15 min.

As exhibited in Figure S2, the TiO₂-B NRs/DA in air-saturated solution (a) exhibited larger photocurrent than that in nitrogen-saturated solution (b), implying the positive effect of dissolved oxygen and the production of cathode photocurrent in this PEC process.

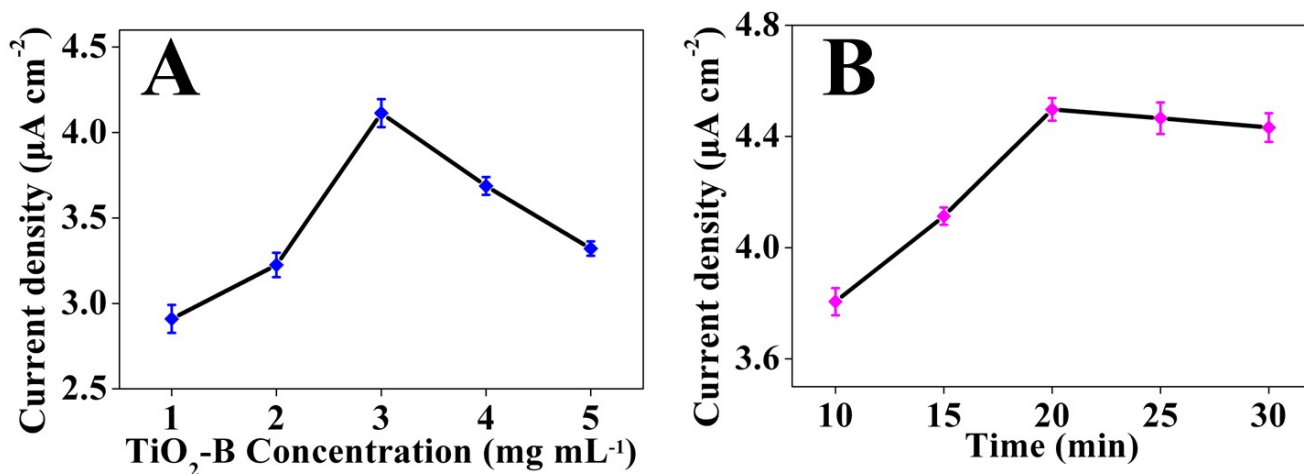


Figure S3. The photocurrent response at (A) different concentration of TiO₂-B NRs and (B) different dipping time of DA of TiO₂-B NRs/DA in pH 7.0 PBS.

The concentration of TiO₂-B NRs is an important parameter relevant to the photocurrent response, thus the PEC performance on different TiO₂-B NRs concentration was investigated in Figure S3A. With the increasing of concentration from 1 mg mL⁻¹ to 5 mg mL⁻¹, the photocurrent density reached a maximum at 3 mg mL⁻¹ and then decreased gradually. This phenomenon was ascribed to that more electrons were excited with the increase of photoactive materials amount, resulting in the enhancement of the photocurrent density. However, the thicker TiO₂-B NRs would gather together, impeding the transfer of the electrons and the effective light harvest. Consequently, 3 mg mL⁻¹ TiO₂-B NRs was selected as the optimized concentration for the signal recording in the following experiments.

To study the effect of DA assembly time on the PEC performance, the photocurrent response at different assembly time was investigated. As exhibited in Figure S3B, the photocurrent density increased upon the increasing of immersion time in 0.015 M of DA from 10 min to 20 min, and then the photocurrent density remained stable. Therefore, considering the optimal analytical performance, the self-assembled time of 20 min was selected in the future study.

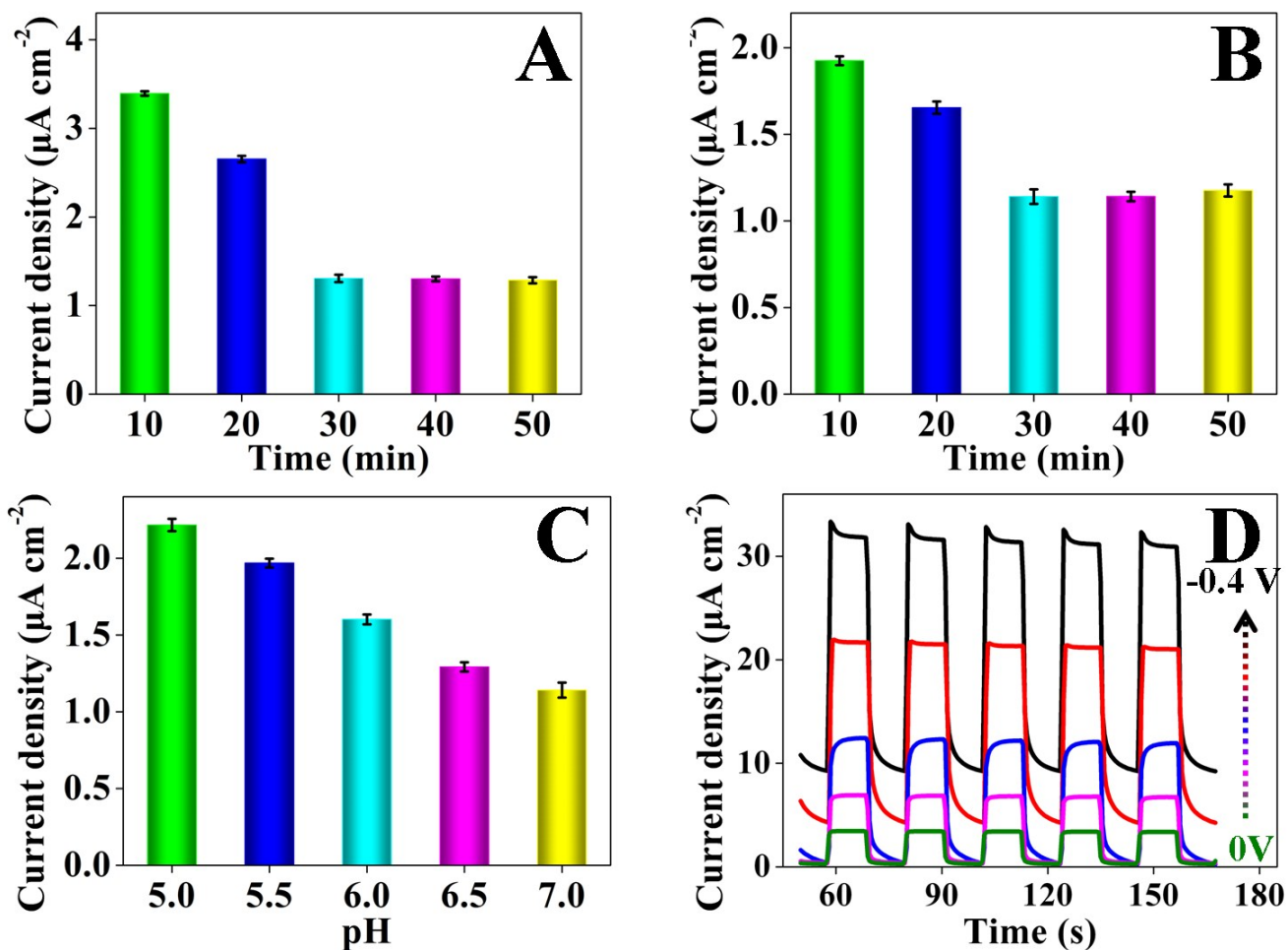


Figure S4. Effects of the incubation time for ConA (A), glucose (B) on the PEC photocurrent in 0.1 M PBS (pH 7.0). Effects of (C) pH and applied potential (D) on photocurrent density.

Due to the fabricated PEC biosensor for glucose determination is closely related to the ConA amount on electrode surface, the photocurrent density on different assembly time of ConA was explored. As displayed in Figure S4A, the photocurrent density reached nearly a plateau after 30 min, indicating the adsorption amount of ConA achieved saturate. Therefore, 30 min was used as the optimal assembly time.

As illustrated in Figure S4B, the relationship between photocurrent density and glucose incubation time was examined in the range from 10 to 50 min. Apparently, the photocurrent density declined quickly with the increasing time then it tended to be constant after 30 min. Considering the determination efficiency, 30 min was chosen as the optimal recognize time between glucose and ConA.

Additionally, the effect of pH was exploited in PBS from 5.0 to 7.0 stepping with 0.5. As presented in Figure S4C, the photocurrent density increases with the decrease of pH. It might be explained that H^+ in acid solution is propitious to the enhancement of cathode photocurrent. Owe to the photocurrent density at pH 6.0 is large enough for the subsequent biosensing, pH 6.0 PBS buffer was selected throughout the subsequent measurements.

The applied potential in this biosensing is another significant influencing parameter relevant to the photocurrent response, the influence of applied potential was evaluated in Figure S4D. The photocurrent density enhanced dramatically with the more negative applied potential from 0 V to -0.4 V, which attributed to an enhancement of the rate constant for charge transfer. In addition, the dark photocurrent of this modified electrode almost negligible from 0 V to -0.2 V, but the high dark photocurrent appeared when more negative applied potential was employed. Therefore, -0.2 V was selected as the applied potential for the glucose determination.

Table S1 Comparison of different methods for glucose detection

Electrode material	Linear ranges (mM)	Detection limit (pg/mL)	Reference
CuONPs-CNFs	0.0005-2.3	0.1	S5
CuONPs-MWCNTs	0.0008-3	0.8	S6
CuONPs-MCs	0.0004-7.3	0.1	S7
TiO ₂ -B NRs/DA	0.00005-1	0.000017	This work

CNFs Carbon nanofibers; MWCNTs Multiwall carbon nanotubes; MCs Mesoporous carbons

Table S2 The results of addition recovery test (n=3)

glucose in sample ($\mu\text{mol L}^{-1}$)	glucose added ($\mu\text{mol L}^{-1}$)	glucose found ($\mu\text{mol L}^{-1}$)	Recovery (%)
56.3	100	153.1	97.9
39.7	80	123.4	103.1
45.8	30	79.3	104.6
73.6	50	118.9	96.2
49.2	40	87.5	98.1

References

- S1 J.J. Feng, P.P. Zhang, A.J. Wang, Q.C. Liao, J.L. Xi and J.R. Chen, *New J. Chem.*, 2012, **36**, 148.
- S2 G.L. Wang, J.J. Xu and H.Y. Chen, *Biosens. Bioelectron.*, 2009, **24**, 2494.
- S3 N.M. Dimitrijevic, Z.V. Saponjic, B.M. Rabatic and T. Rajh, *J. Am. Chem. Soc.*, 2005, **127**, 1344.
- S4 L. de la Garza, Z.V. Saponjic, N.M. Dimitrijevic, M.C. Thurnauer and T. Rajh, *J. Phys. Chem. B*, 2006, **110**, 680.
- S5 J. Zhang, J. L. Ma, S. B. Zhang, W. C. Wang and Z. D. Chen, *Sens. Actuators, B*, 2015, **211**, 385.
- S6 J. Yang, L. C. Jiang, W. D. Zhang and S. Gunasekaran, *Talanta*, 2010, **82**, 25.
- S7 J. Zhang, N. N. Ding, J. Y. Cao, W. C. Wang and Z. D. Chen, *Sens. Actuators, B*, 2013, **178**, 125.